

Tension-clock control of human mitotic chromosome oscillations

Nigel J. Burroughs*

Mathematics Institute, University of Warwick, CV4 7AL. UK.

** Corresponding author: N.J.Burroughs@warwick.ac.uk*

Andrew McAinsh

Warwick Medical School, University of Warwick, CV4 7AL. UK.

During cell division paired (sister) chromosomes are observed to perform approximate saw-tooth oscillations across the cell mid-plane. Experimental data suggests that these oscillations are regulated through intersister tension. We propose a time dependent tension threshold model that exhibits three stable periodic solutions and the phase diagram can be generated semi-analytically. Incorporation of diffusive noise reproduces realistic oscillations, with realistic periods, amplitudes and reproducing the observation that either sister of the pair can switch direction first.

High fidelity cell division in mammals relies on retaining duplicated chromosomes (called chromatids) together in a holding pattern near the cell equator until all paired chromatids are correctly attached to the spindle. In particular, sisters needs to be attached by microtubules to separate spindle poles [1, 2]. Whilst in this holding pattern, chromatid pairs are observed to oscillate parallel to the spindle axis in the majority of animal cells, including humans [3–5]. Oscillations are pseudo-periodic with sections of near constant speed separated by a directional switching event whereby both of the sisters switch direction, Fig. 1A. Oscillations are predictive of segregation errors, [6] and are attenuated in cancer cells [7].

A number of mathematical models of chromosome oscillations have been proposed incorporating various mechanisms, reviewed in [8, 9], oscillations typically arising from mechanical processes [10–14] or chemical feedbacks [15–19]. Microtubules are intrinsically dynamic, exhibiting dynamic instability [20] which provides a natural driver for oscillations. Collective modelling of microtubule binding with force dependent catastrophe/rescue effectively synchronises dynamic instability of the microtubule bundle [10, 12, 14].

However, these tug-of-war models are inconsistent with the low intersister force inferred from data [21], suggesting that directional switching is controlled. The regulatory processes underpinning this control and generates oscillations remain poorly understood, but believed to be a consequence of sister-sister coregulation mediated by tension in the spring-like centromeric chromatin that connects the sisters [5, 22–24]. Sub-pixel 3+1D imaging of kinetochore positions has shown that the two sis-

ters rarely switch coincidentally, with both switching orders being observed, [23]. Specifically the leading sister or the trailing sister can switch first, referred to as leading/trailing sister initiated directional switching, LIDS, TIDS, respectively, [23]. This results in a relaxation (LIDS) or overstretch (TIDS) respectively of the centromeric chromatin spring at a directional switch; i.e. there is a phase where both sisters are attached to polymerising (LIDS), respectively depolymerising (TIDS) microtubules, Fig. 1B, [21]. This raises the question of how control of chromatid direction through the spring tension can give rise to oscillations where both of these states can occur with seemingly little impact on the global oscillation characteristics, including the oscillation period and amplitude. We propose a new mathematical model, formulating the tension clock hypothesis of [23]. It is a force dependent control model, where a dynamic tension threshold controls the time of directional switching of the attached microtubules.

We model the movement of the kinetochores, multi-protein machines that assemble near the middle of each sister chromatid. Kinetochores facilitate the mechanical attachment of the chromosome to a bundle of microtubules, called the K-fiber, that connect the chromatid to one of the spindle poles. K-fiber dynamics is substantially slower than single microtubules, [25, 26]. There are 4 principle forces: a drag force (drag coefficient γ) and an antipoleward polar ejection force (strength α) acting on the chromosomes, a centromeric spring (spring constant κ , natural length L) connecting the sister kinetochores, and a pushing/pulling force f_{\pm} from a polymerising (+), depolymerising (–) attached K-fiber, Fig. 1C. Force balance then give the dynamics, (intersister distance $\Delta = x_1 - x_2$), [21]

$$\begin{aligned}\frac{dx_1}{dt} &= -\frac{f_{\sigma^1(t)}}{\gamma} - \frac{\kappa}{\gamma}(\Delta - L) - \frac{\alpha}{\gamma}x_1 + \sqrt{2D}\xi_1, \\ \frac{dx_2}{dt} &= \frac{f_{\sigma^2(t)}}{\gamma} + \frac{\kappa}{\gamma}(\Delta - L) - \frac{\alpha}{\gamma}x_2 + \sqrt{2D}\xi_2,\end{aligned}\quad (1)$$

where x_1, x_2 are the positions of the two sister kinetochores (normal to the spindle equatorial plane). Sisters are orientated such that $x_1 > x_2$ on average, i.e. sister 1 is attached to the spindle pole to the right, sister 2 to the left. ξ_k are standard white noise modelling thermal and active noise components acting on the kinetochores, parametrised by an effective diffusion coefficient

D. These forces have been inferred from kinetochore tracking data [21, 23], demonstrating that the spring is in low tension throughout the oscillation compared to the dominant force generated by depolymerising microtubules. Sister direction is labelled by $\sigma^k(t) \in \{-, +\}$ for sister $k = 1, 2$. The saw-tooth like oscillations then correspond to a sequence of *coherent* sections where the sisters move in the same direction, one attached to polymerising ($\sigma^k = +$), the other depolymerising ($\sigma^k = -$) microtubules, separated by a fast double switching event where both sisters switch direction (in either order), *i.e.* after the first sister switches there is an *incoherent* section when both sisters are either attached to polymerising (LIDS) or depolymerising (TIDS) microtubules.

The tension-clock hypothesis, [23], provides a mechanism to control directional switching. Analysis of (inferred) force profiles (in HeLa cells, [21, 23], and RPE1 cells [27]) provides evidence of sister direction arising from ageing/degradation of the K-fibre from the time since the last switch. Specifically, polymerising K-fibres are proposed to require increasing pulling forces to remain polymerising, while depolymerising K-fibres have a decreasing load threshold triggering rescue events, Fig. 1C, analogous to observations of yeast kinetochore interactions with single microtubules [28].

We implement the tension-clock dependence as a (linearly) time-varying tension threshold for each K-fibre, a sister switching direction when the spring tension hits its threshold, Fig. 1C. At a switching event we assume a K-fibre is restored to a 'prime' state with tension thresholds T_{pol}^0 , T_{depol}^0 , for polymerising, respectively depolymerising K-fibre, these thresholds then evolve linearly over time (age) $T_{pol}(t) = T_{pol}^0 + a_+(t - t^*)$, $T_{depol}(t) = T_{depol}^0 - a_-(t - t^*)$, where t^* is the time that the sister last switched with rates $a_+, a_- \geq 0$. Thus, a coherent state survives provided $T_{pol}(t) < T(t) < T_{depol}(t)$, with (rescaled) spring tension $T = \kappa(\Delta - L)/\gamma$, and ends when one of these thresholds is reached, thereby switching the associated sister, Fig. 1C. For incoherent states, the sister that previously switched earlier (the older sister) will reach its threshold first. This is a piecewise-smooth dynamical system [29, 30], with reset maps on the threshold switching condition manifolds. Newton's cradle is a familiar exemplar of such a system.

We initially analyse the deterministic version of Eqn. (1) with $D = 0$. We solve Eqns. (1) during sections of constant polymerisation or depolymerisation. The inter-sister distance $\Delta = x_1 - x_2$ decouples,

$$\frac{d\Delta}{dt} = -\frac{(f_{\sigma^1} + f_{\sigma^2})}{\gamma} + 2\frac{\kappa L}{\gamma} - \frac{(2\kappa + \alpha)\Delta}{\gamma}. \quad (2)$$

Between switching events we have the analytical solution $\Delta(t) = \Delta_{\sigma^1\sigma^2}^* (1 - e^{-(2\kappa + \alpha)(t - t^*)/\gamma}) + \Delta_{t^*} e^{-(2\kappa + \alpha)(t - t^*)/\gamma}$, where Δ_{t^*} is the separation at previous switching time t^* . Here $\Delta_{\sigma^1\sigma^2}^* = (2\kappa L - (f_{\sigma^1} + f_{\sigma^2})) / (2\kappa + \alpha)$, corresponding to the steady states for the fixed directional states $\sigma =$

$\{++, +-, --\}$. Since the spring force is a function of Δ only, switching dynamics is only a function of the Δ dynamics.

Periodic solutions can be constructed by suitably combining sections of these solutions through a sequence of states σ , giving oscillatory solutions in the (Δ, T^1, T^2) space, where $T^k(t)$ is the threshold for sister k . Oscillatory solutions are defined by their switching choreography, and the times t_i , $i = 1..n$, of the n sections. There are at least 5 periodic solutions (subscript denoting number of sections), Fig. 2A-C:

1. **LIDS₂ (TIDS₂) oscillation:** an oscillation with LIDS (TIDS) choreography throughout.
2. **BKT₄ oscillation:** Biased kinetochore oscillation where one of the sisters always switches first (alternate LIDS, TIDS events).
3. **Asymmetric LIDS₄ oscillation:** LIDS choreography throughout with asymmetric sections.
4. **Breather**, with anti-correlated sisters.

We performed a stability analysis and bifurcation analysis of these solutions in the a_+, a_- phase plane. These oscillatory solutions occur only in particular regions of the a_+, a_- phase plane, Fig. 2D. TIDS and BKT oscillations are always stable, LIDS₄ unstable and LIDS₂ can be either stable or unstable. The system exhibits standard bifurcations and border collision bifurcations, additional bifurcations of smooth piecewise dynamical systems [29, 30], where the fixed point collides with the switching manifold. Specifically we have the following collision surfaces:

- Σ_{LIDS} . On this surface LIDS₂ and LIDS₄ solutions collide, *i.e.* there are continuations in parameter space for both solutions. This is a standard bifurcation; there is a change in stability of LIDS₂ in a period doubling bifurcation (the period of Δ doubles between LIDS₂ and LIDS₄).
- $\Sigma_{\Delta_{+-}}$. On this surface LIDS₂, TIDS₂ and BKT solutions meet when an incoherent section time $\rightarrow 0$ (a joint switch) and the kinetochores are stationary, $x_{1,2} = \pm\Delta_{+-}/2$ whilst only $T_k(t)$ oscillate. This is a border collision bifurcation where a fixed point collides with the switching manifold [30]; on this surface the threshold conditions change, the sister who switches swops over, *eg* LIDS₂ $\sigma = (+-, ++, -+, ++)$ to TIDS₂ $\sigma = (+-, --, -+, --)$. There is no change in stability.
- $\Sigma_{LIDS_4:BKT}$. On these surfaces a BKT (either sister) and a LIDS₄ solution meet as an incoherent section time $\rightarrow 0$. This is a border collision bifurcation.

A (schematic) bifurcation diagram in a_- , Fig. 2E, summarises the relationship of these solutions and their oscillation format. The period of the oscillations clearly demonstrates the multiple oscillations that exist in various parts of this bifurcation diagram, Fig. 2F.

The breather solution occurs everywhere but is unstable. This is because joint switching is unstable - consider a small perturbation of the breather oscillation that separates the thresholds. When one of the sisters switches its direction, the spring tension moves in the opposite direction, away from the threshold of the second sister.

For human cells the oscillation period is around 70s, and the amplitude of the order of a micron, [21]. The model is able to reproduce such values with a_+, a_- of the order of $10^{-4} \mu\text{m}/\text{s}^2$ (with threshold initialisation $T_{\text{pol}/\text{depol}}^0$ as Fig. 2). The intersister distance Δ oscillates with double the sister oscillation frequency, [4], (as determined by autocorrelation), thus highly asymmetric oscillations BKT_4 are not observed. However, experimentally oscillations that comprise only single types of switching events are rare, and a typical oscillatory trajectory has both LIDS and TIDS events (the LIDS/TIDS ratio depends on cell line, 1.56 [23], 3.76 [21], 2.22 [27]). This indicates system noise is needed as the deterministic oscillations with one type of oscillation choreography (with 0, 50 or 100% LIDS events depending on region) are too uniform in structure.

With diffusive noise, the intersister distance Δ satisfies the Ornstein-Uhlenbeck equation, and the switching time is given by solving a first passage time (FTP) problem with time varying boundaries. No analytical solution for the FPT problem is known in this case, and a numerical method is used [31]. In the presence of diffusive noise we find that the oscillation regions in the phase diagram deteriorate with increasing noise, Fig. 3A-D. At low noise, $D = 10^{-6} \mu\text{m}^2/\text{s}$, the LIDS and KBT regions are essentially intact, but the TIDS region deteriorates with KBT switching (50:50 LIDS/TIDS events) occurring in the proximity of the bifurcation surface. As noise increases the breather oscillation becomes metastable, the breather oscillation being the dominant state in most regions of the phase diagram at high noise $D = 2 \times 10^{-4} \mu\text{m}^2/\text{s}$, Fig. 3C,D, where only the LIDS oscillation remains intact at low a_+ . Trajectories acquire transient periods of breather oscillation at high noise, $D = 2 \times 10^{-4} \mu\text{m}^2/\text{s}$, Fig. 3G. Noise induced stabilisation of unstable structures occurs in other systems [32–35].

This deterioration of saw-tooth like oscillations by noise induced stabilisation of the breather state can be suppressed by preventing switching events occurring too frequently, *i.e.* if there is a reset time t_{ref} after a switching event when further switching of that sister is prohibited. Since the breather state has a short period, this suppresses this state. With a 15s reset period we observe oscillations with a mix of LIDS and TIDS switches and the loss of transient breather states, Fig 3H.

We have presented a new mathematical model of metaphase chromosome oscillations in mammals, where microtubule (bundle) load dependent directional switching is controlled by an ageing threshold, a control mechanism we refer to as the tension-clock. The phase diagram of the deterministic system is derivable semi-analytically. The system displays rich dynamics with at least 5 oscillatory solutions, whilst the unstable breather state is stabilised on introduction of noise. This mechanism reproduces realistic oscillations, in particular reproducing mixed LIDS/TIDS choreographies with realistic amplitudes and periods, Fig. 3H, and has low intersister tension. The next step is to infer the tension-clock parameters from experimental data. Given the semi-Markov nature of the noisy tension-clock model this is challenging.

-
- [1] J. R. McIntosh, M. I. Molodtsov, and F. I. Ataullakhanov, *Quarterly Reviews of Biophysics* **45**, 147 (2012).
 - [2] N. Pavin and I. M. Tolić, *Annual Review of Biophysics* **45**, 279 (2016), pMID: 27145873, <https://doi.org/10.1146/annurev-biophys-062215-010934>.
 - [3] R. V. Skibbens, V. P. Skeen, and E. D. Salmon, *J. Cell Biol.* **122**, 859 (1993).
 - [4] K. Jaqaman, E. M. King, A. C. Amaro, J. R. Winter, J. F. Dorn, H. L. Elliott, N. Mchedlishvili, S. E. McClelland, I. M. Porter, M. Posch, A. Toso, G. Danuser, A. D. McAinsh, P. Meraldi, and J. R. Swedlow, *J. Cell Biol.* **188**, 665 (2010).
 - [5] X. Wan, D. Cimini, L. A. Cameron, and E. D. Salmon, *Mol. Biol. Cell* **23**, 1035 (2012).
 - [6] O. Sen, J. U. Harrison, N. J. Burroughs, and A. D. McAinsh, *Developmental Cell* **56**, 3082 (2021).
 - [7] K. Iemura, Y. Yoshizaki, K. Kuniyasu, and K. Tanaka, *Cancers* **13** (2021), 10.3390/cancers13184531.
 - [8] E. Vladimirou, E. Harry, N. Burroughs, and A. D. McAinsh, *Chromosome Research* **19**, 409 (2011).
 - [9] G. Civelekoglu-Scholey and C. Daniela, *Interface Focus* **4**, 20130073 (2014).
 - [10] A. P. Joglekar and A. J. Hunt, *Biophys* **83**, 42 (2002).
 - [11] G. Civelekoglu-Scholey, B. He, M. Shen, X. Wan, E. Roscioli, B. Bowden, and D. Cimini, *The Journal of Cell Biology* **201**, 577 (2013).
 - [12] E. J. Banigan, K. K. Chiou, E. R. Ballister, A. M. Mayo, M. A. Lampson, and A. J. Liu, *Proceedings of the National Academy of Sciences* **112**, 12699 (2015), <http://www.pnas.org/content/112/41/12699.full.pdf>.
 - [13] A. H. Klemm, A. Bosilj, M. Gluncic, N. Pavin, and I. M. Tolic, *Molecular Biology of the Cell* **29**, 1332 (2018).
 - [14] F. Schwietert and J. Kierfeld, *New Journal of Physics* **22**, 053008 (2020).
 - [15] J. Liu, A. Desai, Jose, N. Onuchic, and T. Hwa, *Proceedings of the National*

- Academy of Sciences **104**, 16104 (2007), <https://www.pnas.org/doi/pdf/10.1073/pnas.0707689104>.
- [16] J. Liu, A. Desai, Jose; N. Onuchic, and T. Hwa, Proceedings of the National Academy of Sciences **105**, 13752 (2008), <https://www.pnas.org/doi/pdf/10.1073/pnas.0807007105>.
- [17] B. Shtylla and J. P. Keener, Journal of Theoretical Biology **263**, 455 (2010).
- [18] J. L. CabreraFernández, G. C. Herrera-Almarza, and E. D. G. M., Physica A: Statistical Mechanics and its Applications **512**, 1121 (2018).
- [19] M. A. C. Medina, K. Iemura, A. Kimura, and K. Tanaka, Biomedical Research **42**, 203 (2021).
- [20] T. Mitchison and M. Kirschner, Nature **312**, 237 (1984).
- [21] J. W. Armond, E. F. Harry, A. D. McAinsh, and N. J. Burroughs, PLOS Computational Biology **11**, 1 (2015).
- [22] C. Rieder and E. Salmon, J. Cell Biol. **124**, 223 (1994).
- [23] N. J. Burroughs, E. F. Harry, and A. D. McAinsh, Elife (2015), 10.7554/eLife.09500.
- [24] F. Rago and I. M. Cheeseman, The Journal of Cell Biology **200**, 557 (2013).
- [25] S. Inoué and E. D. Salmon, Molecular Biology of the Cell **6**, 1619 (1995).
- [26] M. D. Betterton and J. R. McIntosh, Cellular and Molecular Bioengineering **6**, 418 (2013).
- [27] J. U. Harrison, O. Sen, A. D. McAinsh, and N. J. Burroughs, BioRxiv (2021), 10.1101/2021.12.16.472953.
- [28] B. Akiyoshi, K. K. Sarangapani, A. F. Powers, C. R. Nelson, S. L. Reichow, H. Arellano-Santoyo, T. Gonen, J. A. Ranish, C. L. Asbury, and S. Biggins, Nature **468**, 576 (2010).
- [29] M. di Bernardo, C. J. Budd, A. R. Champneys, and P. Kowalczyk, *Piecewise-smooth Dynamical Systems: Theory and Applications* (Springer, 2007).
- [30] O. Makarenkov and J. S. Lamb, Physica D: Nonlinear Phenomena **241**, 1826 (2012), dynamics and Bifurcations of Nonsmooth Systems.
- [31] C. Yi, Quantitative Finance **10**, 957 (2010).
- [32] M. Samoilov, S. Plyasunov, and A. P. Arkin, Proceedings of the National Academy of Sciences **102**, 2310 (2005), <https://www.pnas.org/doi/pdf/10.1073/pnas.0406841102>.
- [33] M. Turcotte, J. Garcia-Ojalvo, and G. M. Süel, Proceedings of the National Academy of Sciences **105**, 15732 (2008).
- [34] P. Rué, G. M. Suel, and J. Garcia-Ojalvo, Physical Review E **83**, 061904 (2011).
- [35] Y. Wu, Y. Jiao, Y. Zhao, H. Jia, and L. Xu, Phys. Rev. E **105**, 014419 (2022).

Figure Legends

Figure 1. The tension-clock model of chromosome oscillations. **A.** Typical oscillatory dynamics of a pair of human kinetochores annotated for LIDS and TIDS, see [23] for methods. **B.** Inferred spring force through a LIDS (magenta, 1614 events) or TIDS (black, 449 events) event, showing relaxation, respectively overstretch of the spring force after the switching event. **C.** Schematic of the tension-clock mechanical model. Chromosome movement is dependent on forces generated by microtubules, [1, 2]. Here a pair of sister kinetochores have microtubule attachments to respective spindle poles. Microtubules, bundled in K-fibres, are assumed to have an evolving threshold, and switch direction if that threshold is met, upper

panel. **A, B** reproduced from [21] with permission.

Figure 2. Dynamic behaviour of the deterministic tension-clock model. Simulations of the tension-clock model showing **A.** Breather state (coincident switching of sisters), **B.** LIDS oscillation, **C.** Biased KT oscillation (BKT, sister 1 always switching). Directional switching events are shown, first sister switching marked with cyan for LIDS, magenta for TIDS. **D.** Trajectories in $x_1 - x_2$ plane. **D.** Phase plot showing existence of LIDS, TIDS and BKT oscillations in the a_+, a_- phase plane. **E.** Bifurcation diagram for a_- constant cross section of D, with schematic of trajectory phase plane (in $x_1 - x_2$). Bifurcations: pitchfork bifurcations, red, purple, border collision bifurcation blue. The solutions continue (dashed) beyond the border surface as unphysical solutions, *i.e.* there is a solution with the same switching choreography but the second sister switches upon the second meeting of the threshold condition (from the wrong direction). **F.** Period of oscillatory solutions with a_- ($a_+ = 5 \times 10^{-4}$; stable oscillations shown with solid lines). Mechanical parameters are set to $f_+/\gamma = 15$ nm/s, $f_-/\gamma = -5$ nm/s, $\kappa/\gamma = 0.025$ s $^{-1}$, $\alpha/\gamma = 0.01$ s $^{-1}$, typical for oscillatory trajectories, [21]. Thresholds are initialised to $T_{pol}^0 = -0.1$ nm/s, $T_{depol}^0 = 12$ nm/s. a_{\pm} in $\mu\text{m}/\text{s}^2$ in **D, E, F.**

Figure 3. The stochastic tension-clock model. **A/C.** Fraction of time that sisters are coherent as a function of the threshold gradients a_{\pm} for **A.** low noise $D = 10^{-6}$ $\mu\text{m}^2/\text{s}$, **C.** high noise $D = 1.25 \times 10^{-4}$ $\mu\text{m}^2/\text{s}$. **B/D.** Fraction of switching events that are LIDS for cases A/C. **E/F/G.** Typical trajectories in the BKT oscillation region of Fig 2D ($a_+ = 3 \times 10^{-4}$, $a_- = 2 \times 10^{-5}$) with increasing diffusive noise: **E.** low diffusive noise $D = 10^{-6}$, **F.** medium diffusive noise $D = 10^{-5}$, **G.** high diffusive noise $D = 10^{-4}$. **H** Stochastic tension-clock model with a reset period of 15 s and other parameters as G. In **E-H** LIDS events are shown in cyan, TIDS in magenta. Other parameters as Fig. 2. a_{\pm} in $\mu\text{m}/\text{s}^2$.

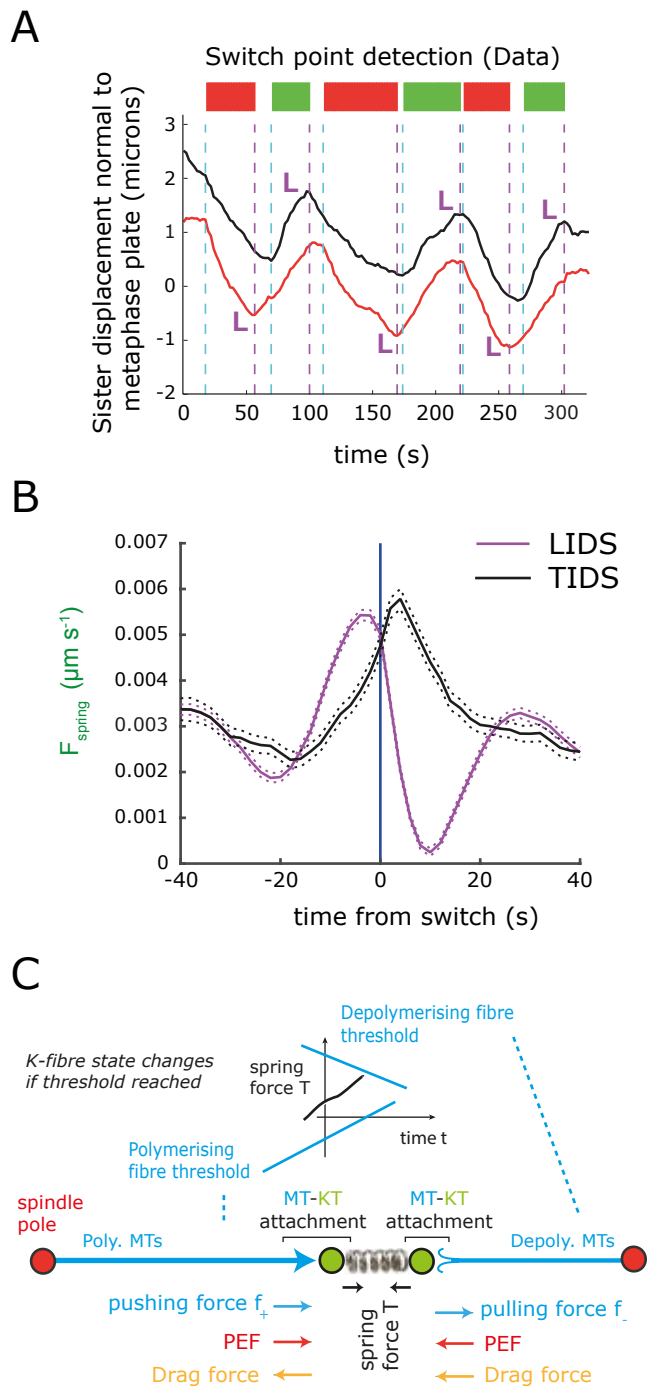


FIG. 1.

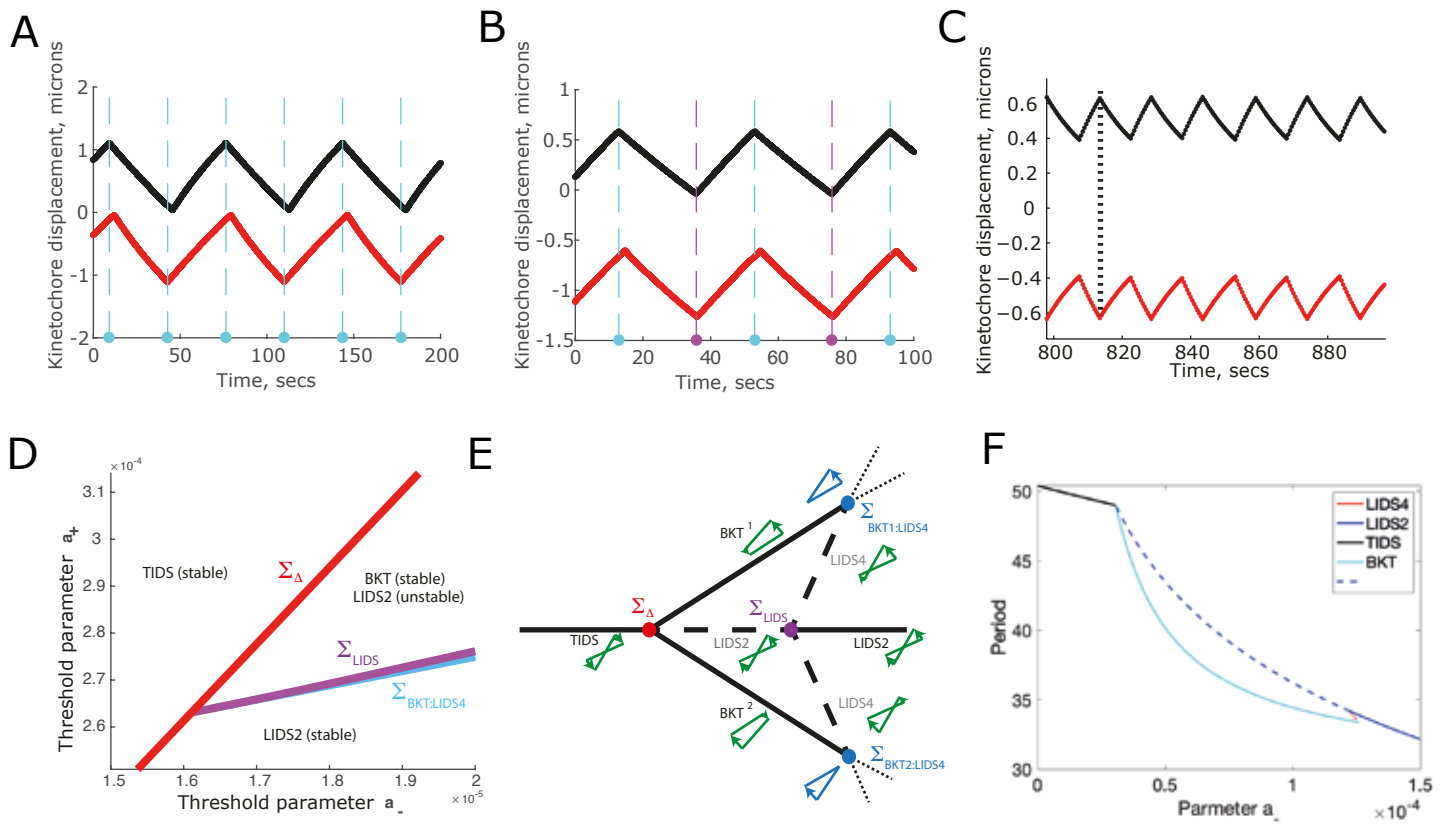


FIG. 2.

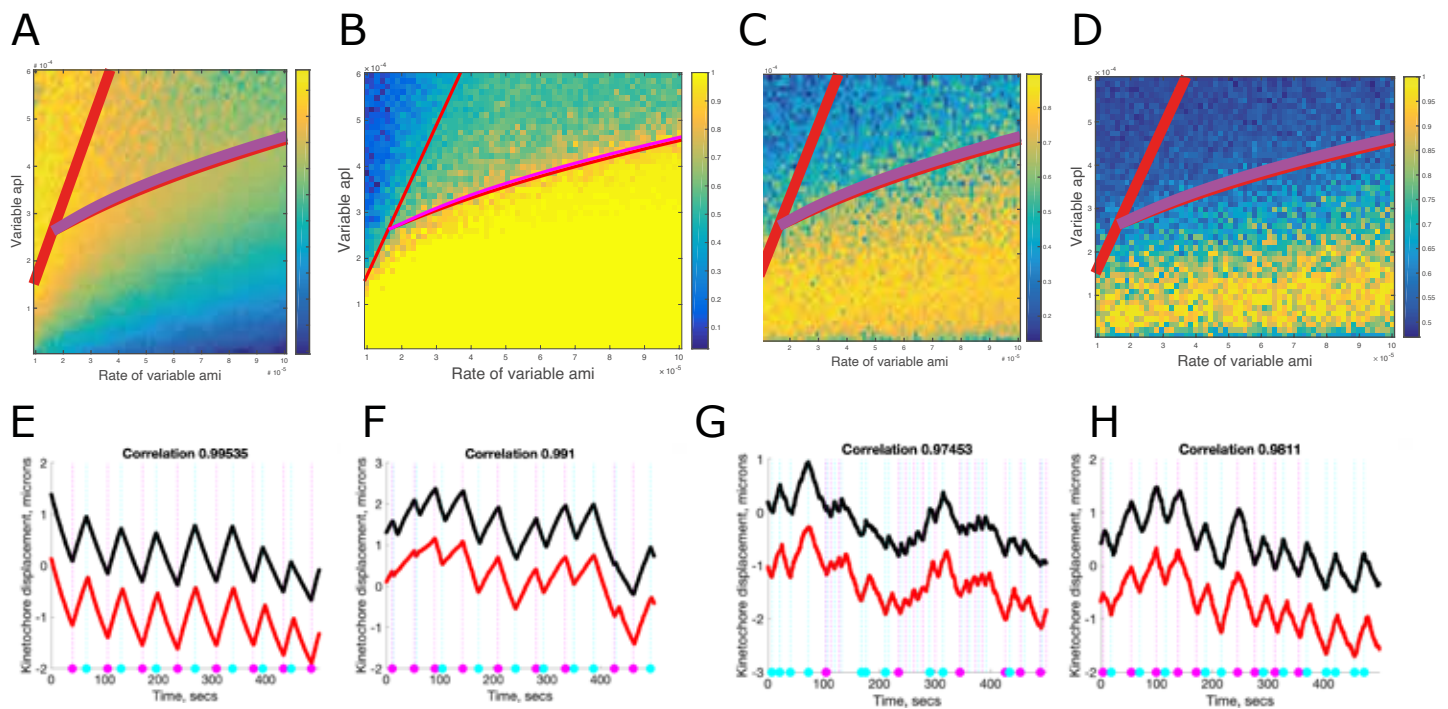


FIG. 3.